Direct 3D Printing of Hybrid Nanofiber-Based Nanocomposites for Highly Conductive and Shape Memory Applications

Hongqiu Wei,[1,2] Xavier Cauchy,[2] Ivonne Otero Navas,[2,3] Yahya Abderrafai,[2] Kambiz Chizari,[2] Uttandaraman Sundararaj,[3] Yanju Liu,[4] Jinsong Leng,*[,1] and Daniel Therriault*[,2]

[1]National Key Laboratory of Science and Technology on Advance Composites in Special Environments, Harbin Institute of Technology, Harbin 150080, People's Republic of China

[2]Laboratory for Multiscale Mechanics, Department of Mechanical Engineering, Polytechnique Montréal, Montreal H3T 1J4, Canada

[3]Polymer Processing Group, Department of Chemical and Petroleum Engineering, University of Calgary, Calgary, Alberta T2N 1N4, Canada

[4]Department of Astronautical Science and Mechanics, Harbin Institute of Technology (HIT), Harbin 150001, People's Republic of China

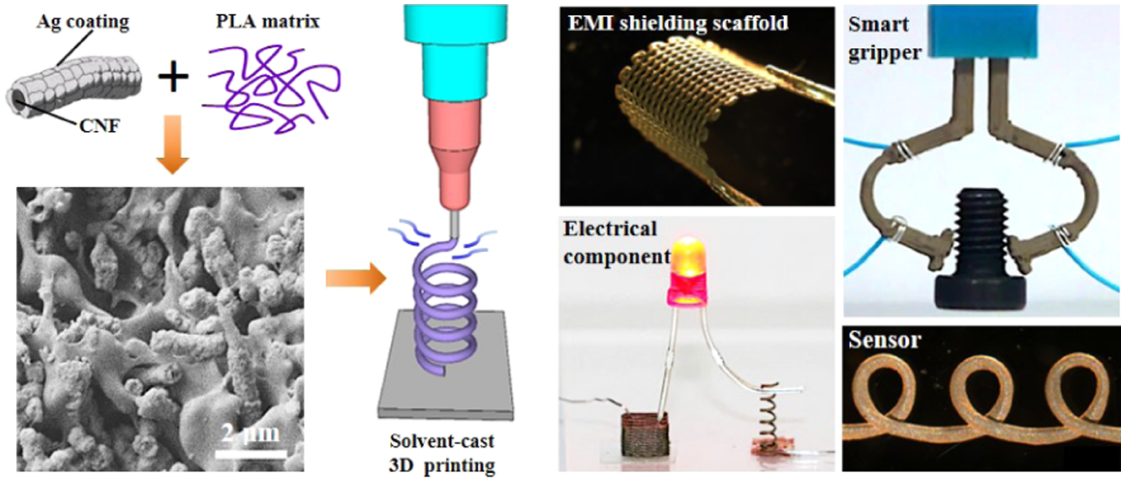

ABSTRACT: Three-dimensional (3D) printing with conductive polymer nanocomposites provides an attractive strategy for the "on-demand" fabrication of electrical devices. This paper demonstrates a family of highly conductive multimaterial composites that can be directly printed into ready-to-use multifunctional electrical devices using a flexible solvent-cast 3D printing technique. The new material design leverages the high aspect ratio and low contact resistance of the hybrid silver-coated carbon nanofibers (Ag@CNFs) with the excellent 3D printability of the thermoplastic polymer. The achieved nanocomposites are capable of printing in open air under ambient conditions, meanwhile presenting a low percolation threshold (i.e., <6 vol %) and high electrical conductivity (i.e., >2.1 × 10^5 S/m) without any post-treatments. We further find that this hybrid Ag@CNF-based nanocomposite shows a quick and low-voltage-triggered electrical-responsive shape memory behavior, making it a great candidate for printing electroactive devices. Multiple different as-printed Ag@CNF-based highly conductive nanocomposite structures used as high-performance electrical devices (e.g., ambient-printable conductive components, microstructured fiber sensors, flexible and lightweight scaffolds for electromagnetic interference shielding, and low-voltage-triggered smart grippers) are successfully demonstrated herein. This simple additive manufacturing approach combined with the synergic effects of the multimaterial nanocomposite paves new ways for further development of advanced and smart electrical devices in areas of soft robotics, sensors, wearable electronics, etc.

KEYWORDS: *3D printing, hybrid nanofiber-based nanocomposites, shape memory, 3D-printed electrical devices, highly conductive applications*

Introduction

Conductive polymer nanocomposites (CPNs) are an important class of functional materials in electronics due to their promising electrical properties, light weight, and adjustable mechanical properties.[1−3] Additive manufacturing, also known as three-dimensional (3D) printing, with CPNs enables one to create electrical structures with highly customized thicknesses, patterns, geometries, etc.[4−9] This technique has been broadly used for building customized and advanced electrical devices, such as liquid sensors,[2,10] radio frequency inductors,[6] high-temperature chambers,[11] nerve conduits,[6] and wearable electronics.[9,12,13] According to the different types of con-

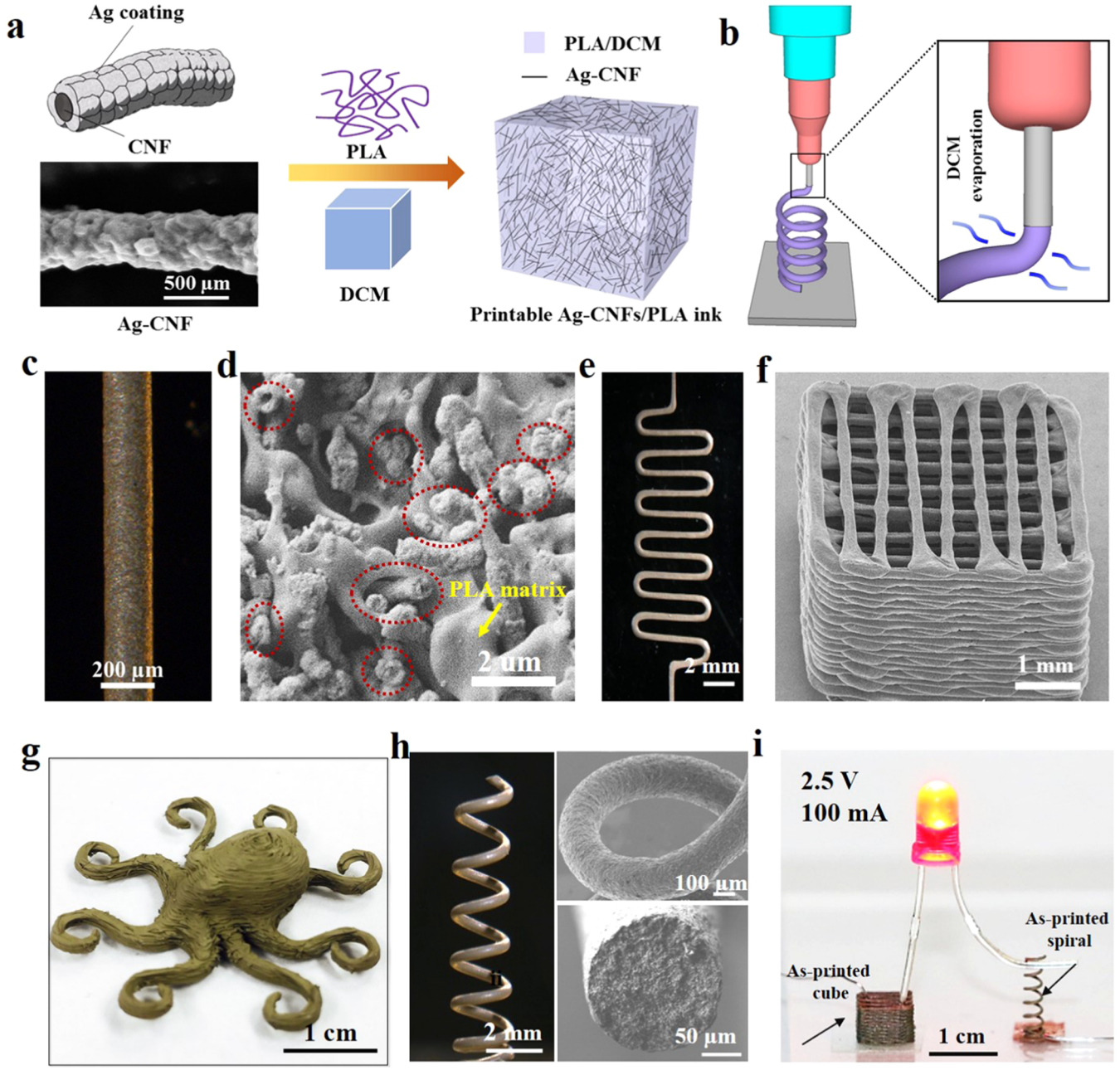

Figure 1. SC printing of Ag@CNF/PLA CPNs. (a) Process of the preparation of SC-printable Ag@CNF/PLA CPNs. (b) Schematic of the SC printing process. (c) As-extruded filament from a nozzle of 200 μm under 1.4 MPa. (d) SEM image of the cross section of a filament (the red circles highlight the circular cross section of the Ag@CNFs). (e–h) SC-printed Ag@CNF/PLA conductive structures ((e) planar zig-zag; (f) simple layer-by-layer 3D cubic scaffold; (g) complicated self-supported 3D octopus; (h) freeform 3D spiral). (i) Demonstration of the conductivity of as-printed structures, showing a cubic scaffold and a spiral connected into a circuit and lightening up a red light-emitting diode (LED) under a voltage of 2.5 V with a current of 100 mA.

ductive fillers, currently reported 3D-printable CPNs can be generally categorized into carbon filler-based CPNs[2,3,6,7,9−11,14−27] and metallic filler (mainly silver filler)-based CPNs.[12,28−33] Carbon fillers, including carbon nanotubes, carbon nanofibers (CNFs), and graphene, are widely known for their low density, high aspect ratio, and theoretically outstanding electrical conductivities.[5,34,35] These properties are advantageous for printing of electrical devices with the desirable properties of a low percolation threshold and light weight. However, the electrical conductivities measured in these CPNs are generally confined to a few thousands of S/m even with a filler loading of up to 62 vol %.[6,7,10,14] The underlying reason for the limited value may be the strong tunneling resistance between individual carbon fillers and the high contact resistance, which relies on the configuration of the neighboring fillers.[36]

Recently, 3D printing with Ag filler (e.g., Ag nanoparticle and Ag flake)-based CPNs has been extensively carried out to construct electrical devices where high conductivity (>10^4 S/m) is indispensable.[12,28−31,33] This approach however requires a very high Ag filler content (>20 vol %) and harsh post-treatments (e.g., high temperature[28−30] or a long curing time[12]) for generating the continuous conductive network. The produced composite structures are generally heavy

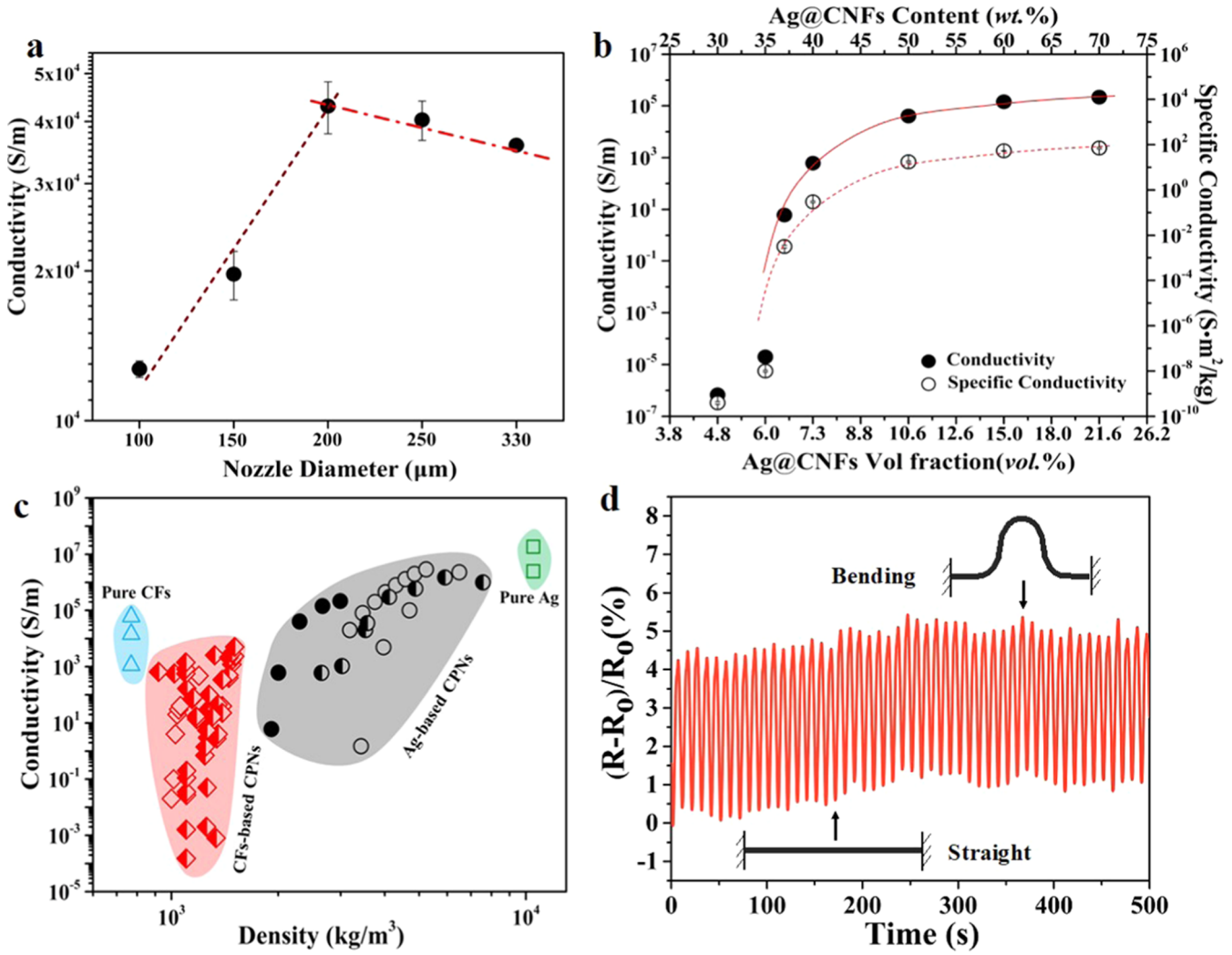

Figure 2. Characterizations of electrical properties of Ag@CNF/PLA CPNs. (a) σ versus nozzle size. (b) σ and specific σ as a function of Ag@CNF loading. (c) Property space map of σ with respect to density that compares our 3D-printable Ag@CNF/PLA CPNs (solid symbols) to other reported 3D-printable CPNs. Open symbols are 3D-printable CPNs that need post-processing. Half-open symbols are 3D-printable CPNs without post-processing. (d) Plot of $(R - R_0)/R_0$ over time during the bending cyclic test of a filament extruded from a nozzle of 200 μm using Ag@CNF CPNs consisting of 10.6 vol % fillers.

(estimated density: 2.6–7.6 g/cm^3)[12,29,30] due to the high density of Ag (10.5 g/cm^3). The usage of Ag nanowires with a high aspect ratio as conductive fillers shows the potential to reduce these shortcomings.[37] However, Ag nanowires are very expensive and involve time-consuming and complicated processes for fabrication and purification.[38,39] Until now, the printing of 3D architectures with superior conductivity and light weight, while being easily processed in open air under ambient conditions without any post-processing, remains difficult to be achieved.

Our strategy in this work is to engineer a 3D-printable, lightweight, and highly conductive nanocomposite by incorporating hybrid nanofibers, namely Ag-coated CNFs (Ag@CNFs), as conductive fillers. Hybrid Ag@CNFs are fabricated by the electroless deposition of Ag onto CNFs.[40] The obtained core–shell configuration enables hybrid Ag@CNFs to integrate the high aspect ratio of CNFs with the high electrical performance (i.e., high conductivity and low contact resistance) of Ag. Meanwhile, the process has no byproduct generated and the Ag@CNFs yielded can be used right after the production without the need for any sort of purification. These advantages indicate that Ag@CNFs are promising nanofillers for building 3D-printable CPNs with highly tunable electrical properties. Herein, we report the design and the one-step 3D printing of hybrid Ag@CNF-based CPNs into customized high-performance electrical devices in open air without any post-treatments. The properties of the nanocomposites are systematically characterized, including their rheological performances, electrical conductivity, and mechanical properties. We further demonstrated different as-printed Ag@CNF-based CPN structures as an electrical component, a microstructured fiber sensor, an electromagnetic interference (EMI) shielding scaffold, and a smart electroactive gripper.

Results and Discussion

The synthesis of Ag@CNFs is presented in Section S1 in the Supporting Information. The scanning electron microscopy (SEM) images in Figure S2 (Supporting Information) show that the achieved Ag@CNFs exhibit a high aspect ratio (>50) and the average thickness of the deposited Ag coatings on the CNFs is ~100 nm. Four-point probe measurements reveal that the electrical conductivity of the Ag@CNF polymer-free film

(i.e., 100 wt % Ag@CNFs) can reach 2.6×10^6 S/m, whereas that for the CNF polymer-free film (i.e., 100 wt % CNFs) is 4.2×10^4 S/m. This improvement of approximately 2 orders of magnitude demonstrates the effectiveness of the Ag coating for enhancing the electrical conductivity. Figure 1a schematically shows the fabrication of the hybrid Ag@CNF-based CPNs. To make Ag@CNFs 3D-printable, thermoplastic poly(lactic acid) (PLA), an ecofriendly polymer with relatively good mechanical properties, is used as a binder. Dichloromethane (DCM) is chosen as a solvent due to its very good PLA dissolvability and fast evaporation. Solvent-cast (SC) printing of Ag@CNF/PLA/DCM CPNs is performed via a computer-controlled pneumatic extrusion of the ink from a micronozzle (Figure 1b). The creation of the solid 3D structure is dependent on the rheological and solvent evaporation behavior of the nanocomposite during printing. Figure S4 (Supporting Information) describes that all Ag@CNF/PLA/DCM CPNs present high process-related viscosities with a pronounced shear thinning behavior. These properties contribute to the easy and stable extrusion of ink at room temperature and prevent the ink from collapsing after extrusion.[41] The solvent evaporation behavior shown in Figure S5 (Supporting Information) reflects that more than 50% of DCM in the nanocomposites evaporates within the first 3 min post-extrusion mainly due to its high vapor pressure (55 kPa). This fast evaporation rate is indispensable for the rapid increase in the rigidity of the extruded filament, which enables the building of solid Ag@CNF/PLA nanocomposite 3D geometries in ambient air.[42] A typical extruded self-supporting cylindrical filament shown in Figure 1c evidences that evaporation of DCM did not cause a significant shrinkage (<5%) to the filament due to the high solid content and the inside rigid Ag@CNF network. The SEM micrograph of the cross section of this filament in Figure 1d shows that hybrid Ag@CNFs are uniformly dispersed in the polymeric matrix. Meanwhile, many circular cross sections of the Ag@CNFs can be clearly observed on the fracture surface, indicating that most Ag@CNFs are oriented along the length of the filament. This phenomenon is attributed to the shear force generated during the uniaxial printing process that induces partial alignment of Ag@CNFs along the flow direction of the filament.[6,30] By simply adjusting the printing parameters (Table S1, Supporting Information), two-dimensional (2D) planar patterns (Figure 1e), 3D cubic scaffolds (Figure 1f), complex irregular bulk 3D shapes (Figure 1g), and even high-quality helical spirals (Figure 1h and Movie S1, Supporting Information) can be directly printed at room temperature in a freeform fashion without the need for any extra support parts, demonstrating the superior 3D printability of Ag@CNF/PLA/DCM nanocomposites.

Electrical properties of the structures are qualitatively observed by connecting an as-printed 3D cubic scaffold and a freeform spiral into a circuit with a red light-emitting diode (LED). Figure 1i shows that the LED can be immediately powered under a voltage of 2.5 V with a current of 100 mA, demonstrating that 3D-printed Ag@CNF/PLA nanocomposite structures are highly conductive and ready to use right after printing. To quantitatively analyze the electrical conductivity (σ), measurements were performed on as-extruded filaments of Ag@CNF/PLA CPNs. Figure 2a shows that the σ along the filament length is inversely proportional to the nozzle diameter for very small nozzles (<200 μm). After reaching the highest conductivity value for a nozzle of 200 μm, the σ slightly decreases with the utilization of larger nozzle diameters. To understand this phenomenon, we also perform a comprehensive characterization of the density and the morphology of these extruded filaments as shown in Figures S6 and S7 in the Supporting Information. We find that the initial elevation of σ is attributed to the fact that the increase of the nozzle diameter from 100 to 200 μm reduces the clogged fibers in the reservoir and increases the quantity of Ag@CNFs coming out of the nozzle (Figure S6a,b, Supporting Information). However, a further increase of the nozzle diameter from 200 to 330 μm reduces the shear rates generated during the extruding process. This lower mechanical shearing probably leads to less alignment of Ag@CNFs along the filament flow direction (Figure S6b,c, Supporting Information)[6,30] and to a slightly lower σ. Figure 2b shows that both σ and specific σ (defined as σ divided by density) of the Ag@CNF/PLA filament extruded from a nozzle of 200 μm increase with the augmentation of the hybrid Ag@CNF loading. The percolation threshold is found to be ~6 vol % (Figure S8, Supporting Information), and the highest σ and specific σ are above 2.1×10^5 S/m and 84 S·m^2/kg, respectively, under a voltage as low as 0.05 V.

As a comparison, we plot the σ of previously reported 3D-printable CPNs together with our results (solid circular symbols) in Figure 2c, and the list of each data point is available in Table S2 (Supporting Information). The σ of Ag@CNF/PLA CPNs are 2−4 orders of magnitude higher than those of all carbon filler-based CPNs[2,6,7,14,16−23,26,27] and even 1−2 orders of magnitude higher than those of pure carbon nanotubes[3] and graphene.[11,15,41] These significant improvements mostly originate from the high σ and low contact resistance between individual fillers provided by the continuous Ag coating in Ag@CNFs. When compared to Ag-based CPNs, our Ag@CNF/PLA CPNs show a much lower percolation threshold (~6 vs ~20 vol %[12,29,30,33]). Ag@CNF/PLA with a filler loading of 10.6 vol % already reaches a conductivity exceeding 10^4 S/m, whereas more than 21 vol % of Ag flakes or Ag nanoparticles[12,29,30,33] are needed to reach the same conductivity. The high aspect ratio (>50) of the wirelike Ag@CNFs facilitates the generation of a continuous conductive network inside the CPNs with lesser filler content, thus enabling a high conductivity while maintaining light weight. Moreover, the σ of Ag@CNF/PLA CPNs with a filler loading of 7.3−21.6 vol % is 6−40 times higher than that of CPNs with the same amounts of Ag flakes or Ag nanoparticles.[10,24,25] Especially, this high σ is achieved without the requirement of either a long curing time or the post-processing reported in other Ag-based 3D-printable CPNs. These conductivity results demonstrate the advantages of the present developed technology for 3D printing of ready-to-use lightweight and highly conductive structures.

The mechanical behavior of our Ag@CNF/PLA nanocomposites was quantitatively evaluated during tensile tests, as shown in Figure S9 in the Supporting Information. With an increasing Ag@CNF content (0−21.6 vol %), Young's modulus (E) of the nanocomposites increases (1.6−2.9 GPa), whereas the elongation at break (ε_b) significantly decreases (17.3−2%). However, the fracture strength (σ_b) of the Ag@CNF/PLA nanocomposite initially starts at 33 MPa (pure PLA), increases to 55 MPa for a concentration of 10.6 vol %, and then drops to 50 MPa for 21.6 vol %. Although not as stretchable as pristine PLA, the highly loaded Ag@CNF/PLA nanocomposites can still be printed to thin conductive structures that are easily bendable. As shown in Movie S2

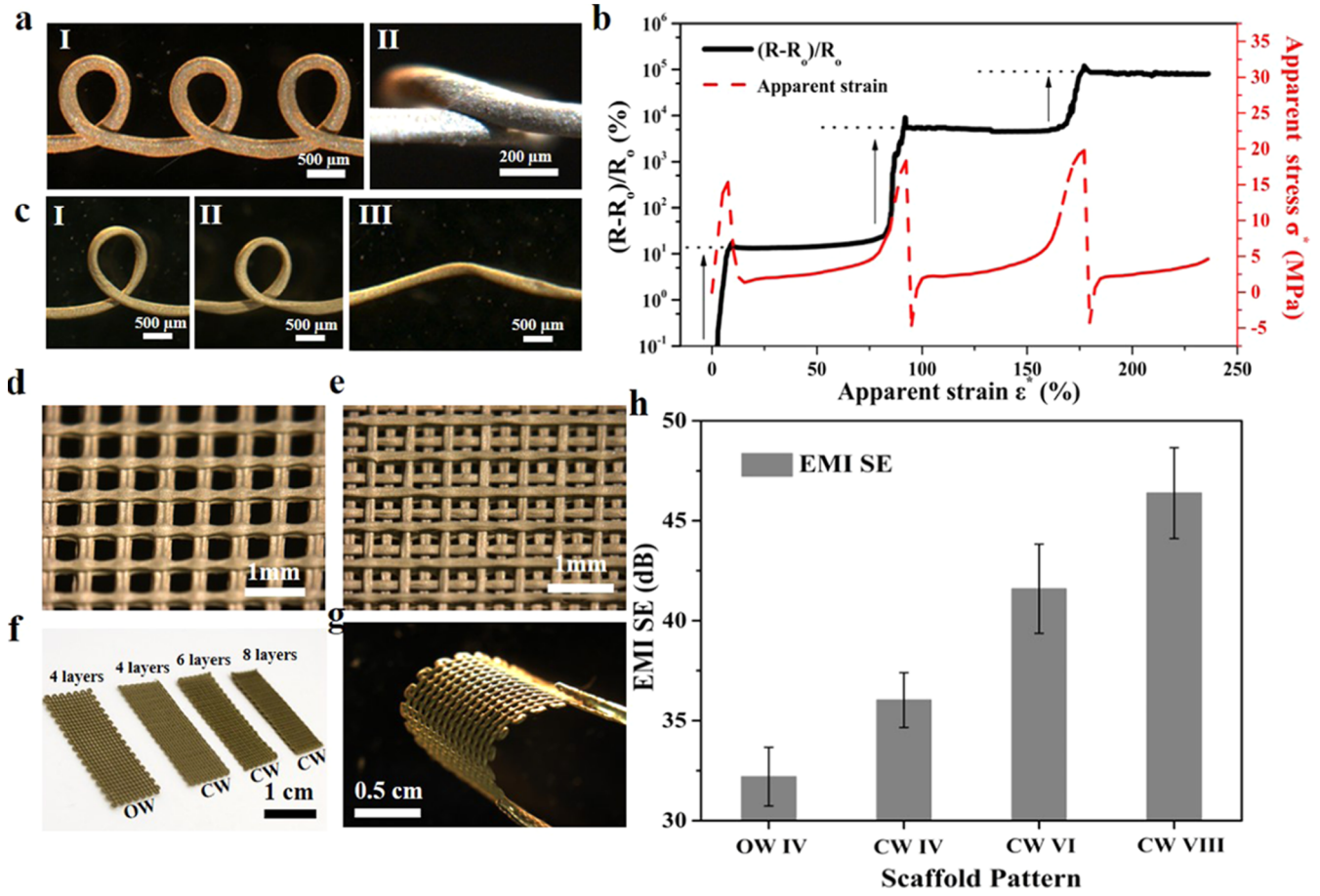

Figure 3. Potential application of 3D-printed highly conductive structures. (a) Morphology of a microstructured fiber: (I) coiled loops; (II) sacrificial bonds. (b) Strain-sensing application of a microstructured fiber with three coiling loops. (c) Illustration of the change during the stretching process: (I, II) breakage of the sacrificial bond; (II, III) release of the hidden length. (d–g) SC-printed conductive scaffolds ((d) OW scaffold; (e) CW scaffold; (f) full view of the OW scaffold with 4 layers and CW scaffold with 4, 6, and 8 layers; (g) a 4-layer OW scaffold bended by tweezers). (h) EMI SE of Ag@CNF/PLA scaffolds with different patterns and thicknesses (OW IV is an OW scaffold with four layers; CW IV, CW VI, and CW VIII are CW scaffolds with 4, 6, and 8 layers, respectively).

(Supporting Information), a single fiber extruded from a nozzle of 200 μm using 10.6 vol % Ag@CNF/PLA nanocomposites could withstand a bending radius as small as 0.6 mm without any damage. We further evaluated the electrical properties of the nanocomposite fiber under mechanical deformation. Figure 2d shows that the variation of normalized resistance ($\Delta R/R$) of the filament in each bending cycle is smaller than 4% throughout 50 cycles and the change in $\Delta R/R$ after the entire cyclic test is minimal (<1%), showing the flexibility of Ag@CNF/PLA nanocomposites, while maintaining their electrical properties.

The enhanced properties of the 3D printing with Ag@CNF/PLA significantly broaden their potential for widespread applications. We chose a Ag@CNF/PLA nanocomposite consisting of 10.6 vol % Ag@CNFs for the demonstration of three applications based on its initial high conductivity (5×10^4 S/m), measured low density (~2 g/cm^3) and moderate mechanical property. First, a 3D-printed Ag@CNF/PLA microstructured fiber fabricated by introducing flow instability during the depositing process (Movie S3, Supporting Information) is used as a strain sensor. According to our previous research,[43] the slenderness ratio H/d_f (H is the distance between the nozzle tip and the platform; d_f is the diameter of the filament) was set at 10 and the speed ratio V_t/V_p (V_t is the extruded speed of the nanocomposite; V_p is the moving speed of the platform) was set at 3 to obtain the desired configuration during the instability-assisted direct-writing process. The obtained microstructured fiber is composed of coiled loops (Figure 3a,I) and sacrificial bonds (Figure 3a,II) located at the overlapping sections. To assess the sensing behavior, a microstructured fiber with three sacrificial bonds was tested in uniaxial tension while monitoring the relative changes in electrical resistance (Movie S4, Supporting Information). Figure 3b shows that its strain–stress curve has a "saw tooth"-like shape. The rapid drops at the stress peaks are caused by the breakage of the sacrificial bonds (Figure 3c,I–II). The plateaus after each peak are corresponding to the release and unfolding of the hidden length in the coiled loops (Figure 3c,II-III). Figure 3b shows the measurements of $\Delta R/R$ during this stretching process, and we observe a stepwise increasing tendency. The breakage of each sacrificial bond induces a sharp increase in $\Delta R/R$ (i.e., 1–2 orders of magnitude), whereas $\Delta R/R$ is relatively stable during the release of the hidden length. This may be attributed to the disappearance of the contact points in the loops, directly resulting in the sudden reduction of conductive paths for the electrons. However, the release of the hidden length does not involve the stretching of the materials (i.e., low stress level), indicating no big influence generated on the distance or space among the conductive fillers. This behavior of the micro-

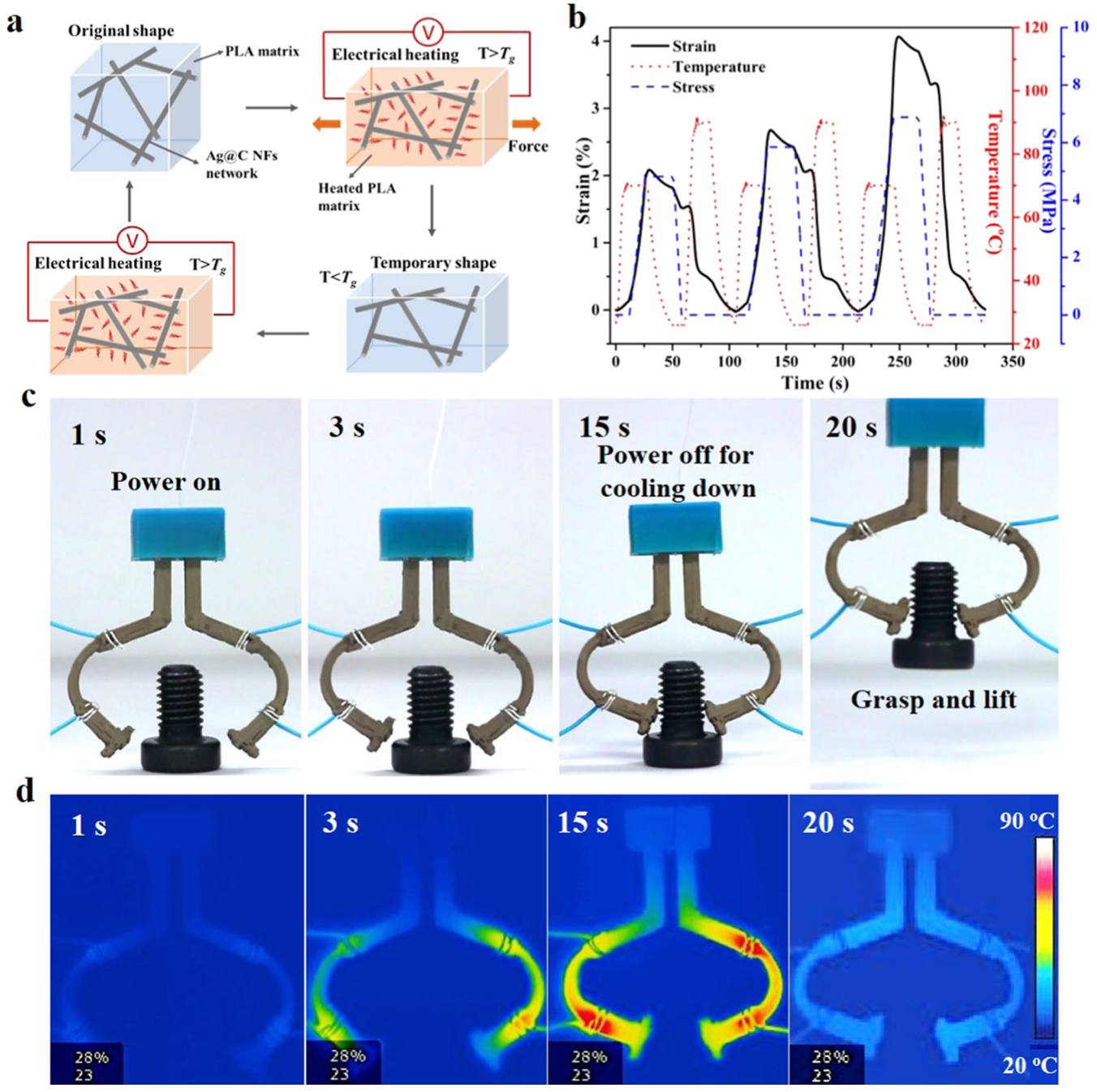

Figure 4. SC printing of an electroactive smart gripper. (a) Schematic of the electroactive shape memory behavior of Ag@CNF/PLA. (b) Shape memory cycles of 10.6 vol % Ag@CNF/PLA with different stretched strains. (c) Snapshots of the electrical-actuated shape-recovery process that leads to the grabbing of a bolt of 5 g. (d) Infrared images of the temperature changes of the gripper during the electrical-actuated shape-recovery process. The testing was carried out under ambient conditions of 23 °C and a humidity of 28%, shown in the left bottom of (d).

structured fiber enables a discontinuous monitoring of strain. Even if the resolution of our microstructured sensor shown here is not as high as that of a typical strain sensor, its performance could be adjusted by a simple change of the number, size, and distance between the coiled loops in the fiber. In addition, the microstructured fiber significantly increases the strain at failure compared to the straight fiber, enabling the monitoring of large strains even when using sensors made of brittle conductive materials.

We also present the use of 3D-printed highly conductive Ag@CNF/PLA scaffolds for functional optimization of electromagnetic interference (EMI) shielding effectiveness (SE). Conductive scaffolds with different patterns (open window (OW) in Figure 3d and closed window (CW) in Figure 3e) and thicknesses (4, 6, and 8 layers) are successfully designed and printed (Figure 3f). These 3D-printed gridlike conductive scaffolds are thin and flexible. Figure 3g shows that a four-layer OW scaffold (thickness: ~350 μm) can be easily bended to nearly 180° without breakage. EMI shielding results over the X-band frequency range (8.2−12.4 GHz) in Figure 3h reveal that the change of the structural pattern from OW to CW directly results in a 12.5% increase in the EMI SE (eqs S2−S4, Supporting Information). This difference might be due to the larger air gaps in the printed pattern of OW in

comparison with those in the CW scaffold. As the number of layers increases from two to eight in CW scaffolds, EMI SE elevates from 36 to 46 dB. The improvement is due to the fact that the increased number of layers provide more conductive paths for carrying free charges. These results indicate that the EMI SE is easily and conveniently adjustable by a simple change of the printing configuration of the scaffolds instead of conventionally changing the nanocomposite compositions. We further compared the EMI SE of our Ag@CNF/PLA scaffolds to that of CNF/PLA scaffolds (i.e., without the silver coating on the fillers). Figure S10 in the Supporting Information shows that the EMI SE and the specific EMI SE (eq 1 in the Experimental Section) of the six-layer CW CNF/PLA scaffold with 10.6 vol % CNF loading are 24.4 dB and 39.7 dB/(g·cm^3), respectively. These values are 57 and 22.5% lower than those of Ag@CNF/PLA scaffolds for the same configuration (i.e., 6-layer CW and 10.6 vol % Ag@CNF loading). The 3D-printed highly conductive Ag@CNF/PLA nanocomposite scaffold appears to provide enhanced EMI SE.

Besides the aforementioned performances, another important advantage of the high conductivity is to provide the Ag@CNF/PLA nanocomposite with a highly efficient Joule heating effect under low voltage. Meanwhile, the addition of wirelike Ag@CNFs into the PLA probably brings a high shape memory behavior to the nanocomposite. It was demonstrated that high entanglements between two materials can effectively reduce the irreversible intermolecular slippages under thermomechanical conditions and lead to the important shape memory behavior.[44,45] Based on the above two characteristics, we assume that the Ag@CNF/PLA nanocomposite could present a very strong electroactive shape memory performance, meaning that the material could actively return to its original shape after undergoing a change to a temporary deformed configuration under Joule heating produced by electrical energy (schematically shown in Figure 4a). The dynamic thermomechanical analysis in Figure S11 (Supporting Information) verifies that the Ag@CNF/PLA nanocomposite experiences obvious glass transition at around 80.5 °C. The shape memory cycles (defined in Section S9 in the Supporting Information) in Figure 4b quantitatively reflect that the shape-recovery ratios (R_r: calculated per eq S5 in the Supporting Information) of our Ag@CNF/PLA nanocomposite under different tensile strains are all above 99%, which is an improvement of 12.5% compared to that of pure PLA (Figure S12, Supporting Information). Figure S13 and Movie S5 in the Supporting Information show that a scaffold printed with 10.6 vol % Ag@CNF/PLA nanocomposite could actively return to its as-printed straight shape from the temporary spiral configuration under 80 °C, demonstrating a high shape memory behavior.

The observed shape memory behavior combined with the high conductivity of the Ag@CNF/PLA nanocomposite enables the utilization of our Ag@CNF/PLA nanocomposite for one-step printing of electroactive devices. A smart gripper is given here as an example. Figure S14a (Supporting Information) shows the design of the gripper. When the curved sections of the two fingers of the gripper are connected to a 1 V, 0.1 A power source, the open gripper (Figure S14b), the material of which is already programmed (see Section S10 in the Supporting Information for the material-programming process), can gradually recover to the closed configuration, presenting an active shape-changing behavior. Figure 4c and Movie S6 (Supporting Information) show that this recovery process enables the gripper to automatically grab a bolt of 5 g in 20 s. The temperature evolution on the surface of the gripper during the shape-changing process is monitored by an infrared (IR) camera. In Figure 4d, we find that the temperature can quickly increase to 80 °C (15 s) with a rather uniform distribution under a voltage of 1 V and then drops to room temperature in ∼5 s after the voltage is removed. These variations are attributed to the high conductivity of the Ag@CNF/PLA nanocomposite enabling rapid and efficient Joule heating inside the printed structures. The low-voltage (1 V)-triggered fast electroactive behavior (i.e., memory effect) of our one-step 3D-printed Ag@CNF/PLA nanocomposite structures is much more advantageous than other actuation methods (e.g., ovens[46,47] and high electrical voltages (>20 V)[19,48,49]) for electronic applications where the power source is limited.

Conclusions

In summary, we have successfully designed a novel kind of ambient-printable CPNs consisting of hybrid Ag@CNFs as conductive fillers, thermoplastic PLA as the matrix, and DCM as the solvent. These hybrid nanofiber-based CPNs could be directly manufactured into various geometries without the usage of any supports, including one-dimensional, 2D, layer-by-layer, and freeform 3D structures, in open air using the SC printing technique. The printed structures present a percolation threshold under 6 vol % (35 wt %) and a σ above 2.1 × 10^5 S/m without any post-treatments. We have successfully demonstrated that 3D-printed Ag@CNF/PLA CPN structures can be directly used for various demanding applications, including electrical components, strain sensors, and EMI shielding scaffolds. Moreover, the integration of the high σ of hybrid Ag@CNFs with the shape memory behavior with PLA enables us to achieve printing of electroactive structures. A printed smart gripper triggered with a voltage as low as 1 V was successfully demonstrated herein. During our printing experiments, we also observed that our Ag@CNF/PLA nanocomposites showed very strong adhesion with various substrates including poly(ethylene terephthalate) and poly(methyl methacrylate). This strong adhesion is probably due to the residual DCM solvent in the Ag@CNF/PLA nanocomposite, which could partially dissolve the top surface of the substrates. In a future study, we plan to investigate the utilization of our Ag@CNF/PLA nanocomposites for flexible electronics where the adhesion between the printed structures and substrates will be even more important. We believe that direct 3D printing with the hybrid Ag@CNF-based CPNs developed herein is promising for the "on-demand" design and construction of a wide array of superior conductive, lightweight, and "active" (i.e., shape memory) electrical devices for more advanced applications in areas ranging from electronics to aerospace and beyond.

Experimental Section

Conductive Ink Fabrication: The hybrid Ag@CNFs were fabricated following the experimental procedure developed by Cauchy et al.[40] The synthesis process of the Ag@CNFs is explained in detail in Section S1 (Supporting Information). To prepare the Ag@CNF/PLA ink, as-received PLA pellets were dried in a vacuum oven for 24 h at 50 °C to remove the moisture. DCM (purity of 99%) was used as the solvent to mix PLA and Ag@CNFs. Ag@CNF/PLA nanocomposite inks with different concentrations were fabricated by thoroughly mixing 2 g of Ag@CNFs, different amounts of PLA (4.67,

3.71, 3.40, 3, 2, 1.33, 0.85, and 0.5 g), and DCM (the weight ratio of PLA to DCM was 1/10) in a sealed container. The mixture was magnetically stirred at a speed of 300 rpm for 3 h, followed by stirring at 800 rpm for 2 h. The container was then kept open for the evaporation of DCM under continuous stirring. During this procedure, the stirring rate was adjusted according to the increased viscosity of solutions. The Ag@CNF/PLA inks were achieved when the weight ratio of PLA/DCM was 1/3. All of the procedures were performed at room temperature. The obtained inks were stored in sealed containers until printing.

SC Printing: The SC printing assembly consisted of three parts: a deposition robot (I&J2200-4, I&J Fisnar) that can move along the x, y, and z axes under the control of a commercial software (JR Points for Dispensing, Janome Sewing Machine), an adjustable air pressure supply (Ultra 2400, EFD), and a high-pressure dispensing apparatus (HP-7x, EFD). For printing, the prefabricated ink was first transferred into a 3 mL syringe (EFD) using a spatula. This syringe with the desired nozzle was then put into the HP-7x apparatus, which was connected to a pressure supply. Next, the HP-7x adaptor with the syringe was mounted on the head of the robot. The ink was extruded from the nozzle upon application of air pressure. User-defined geometries were printed by accurate control of the applied pressure, direction, and velocity of the robot. The detailed printing parameters of each structure can be found in Table S1 (Supporting Information).

Electrical Conductivity Characterization: Ag@CNF/PLA with a filler loading of 10.6 vol % was extruded from nozzles with various inner diameters to investigate the effects of the nozzle size on the σ. Ag@CNF/PLA nanocomposites with different filler loadings were extruded from a nozzle of 200 μm to study the relationship between the loading of conductive fillers and the σ. The extruded filaments were cut to 10 mm length for electrical measurements. Optical microscopy (BX-61, Olympus) was used to film the filament, and the diameter of each filament was measured using Image J software. The electrical measurements were performed on a two-probe testing assembly with a digital multimeter (6517B, Keithley, Kickstart Software), with copper tape pasted on the two ends of the filament. The resistance measurement of each filament was achieved along the extruded direction at room temperature under a voltage of 0.05 V. Five filaments were measured for each test.

Cyclic Mechanical Testing: Filaments extruded from a nozzle of 200 μm with a length of 50 mm using 10.6 vol % Ag@CNF/PLA were subjected to cyclic mechanical testing. The experiment was carried out on a tensile fixture (Insight 50, MTS), and the displacement between the upper and lower clamps is 30 mm. The initial electrical resistance (R_0) was recorded before testing. Then, the upper clamp moved 20 mm toward the lower clamp to flex the filament. After that, the upper clamp was moved back to straighten the filament. This process was repeated for 50 cycles. The real-time electrical resistance (R) during this process was recorded by a digital multimeter (6517B, Keithley, Kickstart Software).

Fabrication and Characterization of the Microstructured Fiber Sensor: The microstructured fiber was fabricated by extruding the 10.6 vol % Ag@CNF/PLA ink from a nozzle of 200 μm at 1 mm/s robot velocity under 0.42 MPa. The uniaxial tensile test was performed on a tensile test machine (Insight 50, MTS) at a strain rate of 5 mm/min. The R value was monitored by a digital multimeter (6517B, Keithley, Kickstart Software) until the fiber was broken.

Fabrication and Characterization of Scaffolds for EMI Shielding: Conductive scaffolds with an area of 15 mm × 30 mm were printed using 10.6 vol % Ag@CNF/PLA under 0.7 MPa at 5 mm/s and a nozzle of 200 μm. The space between every two filaments was set as 0.7 mm. For the OW configuration, filaments of the third and fourth layers were deposited exactly overlapping those of the first and second layers. For the CW configuration, filaments were printed intercalated. EMI SE was measured by an E5071C network analyzer (Agilent) over the X-band frequency range (8.2−12.4 GHz). The detailed testing methods are available in Section S7 in the Supporting Information. The specific EMI SE was obtained by the following equation

$$\text{specific EMI SE} = \frac{\text{EMI SE}\cdot V}{m} \quad (1)$$

where m is the mass of the as-printed scaffold and V is the structural volume including the empty space.[6]

Fabrication and Characterization of the Electrically Actuated Four-Dimensional Gripper: The gripper was printed by a nozzle of 250 μm at 10 mm/s under 0.7 MPa. The shape-changing and shape-recovery processes were carried out under a voltage of 1 V using a commercial power supply.

Microstructure and Structure Characterization: The morphologies of the printed structures obtained by a scanning electron microscope (SEM) (JSM-7600F, JEOL. Ltd.) were first sputtered with gold for 15 s and observed at 10 kV. Optical images of the printed structures were observed using an optical microscope (BX-61, Olympus).

Supporting Information

The Supporting Information is available free of charge on the ACS Publications website at DOI: 10.1021/acsami.9b04245.

SC printing of Ag@CNFs/PLA nanocomposite freeform 3D spiral (AVI)

Cyclic bending test of a Ag@CNFs/PLA nanocomposite fiber extruded from a nozzle of 200 μm (AVI) Fabrication of the Ag@CNFs/PLA nanocomposite microstructured fiber (AVI) Uniaxial tensile test of a Ag@CNFs/PLA nano-composite microstructured fiber with three coiling (AVI)

Shape recovery process of an SC-printed scaffold (AVI) Electrical-actuated gripping process of Ag@CNFs/PLA nanocomposite gripper (AVI)

SC printing, cyclic bending test, fabrication, and uniaxial tensile test of the Ag@CNF/PLA nanocomposite fiber; shape-recovery process of an SC-printed scaffold; electrical-actuated gripping process of the nanocompo-site gripper; and full experimental details, including characterization of the described materials (PDF)

Corresponding Authors

*E-mail: lengjs@hit.edu.cn (J.L.).
*E-mail: daniel.therriault@polymtl.ca (D.T.).

ORCID

Hongqiu Wei: 0000-0002-4842-3390
Jinsong Leng: 0000-0001-5098-9871
Daniel Therriault: 0000-0002-4456-9472

Author Contributions

This manuscript was written through contributions of all authors. All authors have given approval to the final version of the manuscript.

Notes

The authors declare no competing financial interest.

Acknowledgements

The work was financially supported by the Natural Sciences and Engineering Research Council of Canada (NSERC), National Natural Science Foundation of China (Grant No. 11632005, 11672086), and the Foundation for Innovative Research Groups of the National Natural Science Foundation of China (Grant No. 11421091), for which the authors are very grateful. H.W. would also like to thank the Chinese

Scholarship Council (CSC) for funding her research work at Polytechnique Montréal.

References

(1) Chun, K. Y.; Oh, Y.; Rho, J.; Ahn, J. H.; Kim, Y. J.; Choi, H. R.; Baik, S. Highly Conductive, Printable and Stretchable Composite Films of Carbon Nanotubes and Silver. *Nat. Nanotechnol.* **2010**, *5*, 853.

(2) Guo, S.; Yang, X.; Heuzey, M. C.; Therriault, D. 3D Printing of a Multifunctional Nanocomposite Helical Liquid Sensor. *Nanoscale* **2015**, *7*, 6451−6456.

(3) Shin, S. R.; Raziyeh, F.; Ali, T.; Vijayan, M.; Pooria, M.; Shrike, Z. Y.; Mohsen, A.; Mi, J. S.; Duckjin, K.; Mattia, C.; Nasim, A.; Ebrahim, A. H. F.; Dokmeci, M. R.; Ali, K. A Bioactive Carbon Nanotube-based Ink for Printing 2D and 3D Flexible Electronics. *Adv. Mater.* **2016**, *28*, 3280−3289.

(4) Kamyshny, A.; Magdassi, S. Conductive Nanomaterials for 2D and 3D Printed Flexible Electronics. *Chem. Soc. Rev.* **2019**, 1712−1740.

(5) Farahani, R. D.; Dubé, M.; Therriault, D. Three-dimensional Printing of Multifunctional Nanocomposites: Manufacturing Techniques and Applications. *Adv. Mater.* **2016**, *28*, 5794−5821.

(6) Jakus, A. E.; Secor, E. B.; Rutz, A. L.; Jordan, S. W.; Hersam, M. C.; Shah, R. N. Three-Dimensional Printing of High-content Graphene Scaffolds for Electronic and Biomedical Applications. *ACS Nano* **2015**, *9*, 4636−4648.

(7) Kim, J. H.; Lee, S.; Wajahat, M.; Jeong, H.; Chang, W. S.; Jeong, H. J.; Yang, J. R.; Kim, J. T.; Seol, S. K. Three-dimensional Printing of Highly Conductive Carbon Nanotube Microarchitectures with Fluid Ink. *ACS Nano* **2016**, *10*, 8879−8887.

(8) Lewis, J. A.; Ahn, B. Y. Three-dimensional printed electronics. *Nature* **2015**, *518*, 42.

(9) Chen, S.; Huang, T.; Zuo, H.; Qian, S.; Guo, Y.; Sun, L.; Lei, D.; Wu, Q.; Zhu, B.; He, C.; Mo, X.; Jeffries, E.; Yu, H.; You, Z. A Single Integrated 3D-Printing Process Customizes Elastic and Sustainable Triboelectric Nanogenerators for Wearable Electronics. *Adv. Funct. Mater.* **2018**, *28*, No. 1805108.

(10) Chizari, K.; Daoud Mohamed, A.; Ravindran Anil, R.; Therriault, D. 3D Printing of Highly Conductive Nanocomposites for the Functional Optimization of Liquid Sensors. *Small* **2016**, *12*, 6076−6082.

(11) Yao, Y.; Fu, K. K.; Yan, C.; Dai, J.; Chen, Y.; Wang, Y.; Zhang, B.; Hitz, E.; Hu, L. Three-dimensional Printable High-temperature and High-rate Heaters. *ACS Nano* **2016**, *10*, 5272−5279.

(12) Guo, S. Z.; Qiu, K.; Meng, F.; Park Sung, H.; McAlpine Michael, C. 3D Printed Stretchable Tactile Sensors. *Adv. Mater.* **2017**, *29*, No. 1701218.

(13) Kim, C.; Ahn, B. Y.; Wei, T. S.; Jo, Y.; Jeong, S.; Choi, Y.; Kim, I. D.; Lewis, J. A. High-Power Aqueous Zinc-Ion Batteries for Customized Electronic Devices. *ACS Nano* **2018**, *12*, 11838−11846.

(14) Chizari, K.; Arjmand, M.; Liu, Z.; Sundararaj, U.; Therriault, D. Three-dimensional Printing of Highly Conductive Polymer Nanocomposites for EMI Shielding Applications. *Mater. Today Commun.* **2017**, *11*, 112−118.

(15) Kim, J. H.; Suk, C. W.; Daeho, K.; Ryul, Y. J.; Tark, H. J.; Lee, G. W.; Tae, K. J.; Kwon, S. S. 3D Printing of Reduced Graphene Oxide Nanowires. *Adv. Mater.* **2014**, *27*, 157−161.

(16) Zhang, D.; Chi, B.; Li, B.; Gao, Z.; Du, Y.; Guo, J.; Wei, J. Fabrication of Highly Conductive Graphene Flexible Circuits by 3D Printing. *Synth. Met.* **2016**, *217*, 79−86.

(17) Christ, J. F.; Aliheidari, N.; Ameli, A.; Pötschke, P. 3D Printed Highly Elastic Strain Sensors of Multiwalled Carbon Nanotube/Thermoplastic Polyurethane Nanocomposites. *Mater. Des.* **2017**, *131*, 394−401.

(18) Postiglione, G.; Natale, G.; Griffini, G.; Levi, M.; Turri, S. Conductive 3D Microstructures by Direct 3D Printing of Polymer/Carbon Nanotube Nanocomposites via Liquid Deposition Modeling. *Composites, Part A* **2015**, *76*, 110−114.

(19) Rodriguez, J. N.; Zhu, C.; Duoss, E. B.; Wilson, T. S.; Spadaccini, C. M.; Lewicki, J. P. Shape-morphing Composites with Designed Micro-architectures. *Sci. Rep.* **2016**, *6*, No. 27933.

(20) Leigh, S. J.; Bradley, R. J.; Purssell, C. P.; Billson, D. R.; Hutchins, D. A. A Simple, Low-cost Conductive Composite Material for 3D Printing of Electronic Sensors. *PLoS ONE* **2012**, *7*, No. e49365.

(21) Lebel, L. L.; Brahim, A.; El, K. M. A.; Therriault, D. Ultraviolet-assisted Direct-write Fabrication of Carbon Nanotube/Polymer Nanocomposite Microcoils. *Adv. Mater.* **2009**, *22*, 592−596.

(22) Tabiai, I.; Hughes, V.; Chizari, K.; Therriault, D. 3D Printable Conductive Nanocomposites of PLA and Multi-walled Carbon Nanotubes. *Tech. Rep.* **2016**, 61−63.

(23) Gnanasekaran, K.; Heijmans, T.; van Bennekom, S.; Woldhuis, H.; Wijnia, S.; de With, G.; Friedrich, H. 3D Printing of CNT- and Graphene-based Conductive Polymer Nanocomposites by Fused Deposition Modeling. *Appl. Mater. Today* **2017**, *9*, 21−28.

(24) Composite PLA - Electrically Conductive Graphite. https://www.proto-pasta.com/products/conductive-pla?variant=1265211476.

(25) Conductive Graphene PLA Filament. http://www.blackmagic3d.com/Conductive-p/grphn-pla.htm.

(26) Mohan, V. B.; Krebs, B. J.; Bhattacharyya, D. Development of Novel Highly Conductive 3D Printable Hybrid Polymer-graphene Composites. *Mater. Today Commun.* **2018**, *17*, 554−561.

(27) Mu, Q.; Wang, L.; Dunn, C. K.; Kuang, X.; Duan, F.; Zhang, Z.; Qi, H. J.; Wang, T. Digital Light Processing 3D Printing of Conductive Complex Structures. *Addit. Manuf.* **2017**, *18*, 74−83.

(28) Lee, S.; Kim, J. H.; Wajahat, M.; Jeong, H.; Chang, W. S.; Cho, S. H.; Kim, J. T.; Seol, S. K. Three-dimensional Printing of Silver Microarchitectures Using Newtonian Nanoparticle Inks. *ACS Appl. Mater. Interfaces* **2017**, *9*, 18918−18924.

(29) Jo, Y.; Kim, J. Y.; Kim, S. Y.; Seo, Y. H.; Jang, K. S.; Lee, S. Y.; Jung, S.; Ryu, B. H.; Kim, H. S.; Park, J. U.; Choi, Y.; Jeong, S. 3D-printable, Highly Conductive Hybrid Composites Employing Chemically-reinforced, Complex Dimensional Fillers and Thermoplastic Triblock Copolymers. *Nanoscale* **2017**, *9*, 5072−5084.

(30) Valentine, A.; Busbee, T.; Boley, J. W.; Raney, J.; Chortos, A.; Kotikian, A.; Berrigan, J. D.; Durstock, M.; Lewis, J. Hybrid 3D Printing of Soft Electronics. *Adv. Mater.* **2017**, *29*, No. 1703817.

(31) Skylar-Scott, M. A.; Gunasekaran, S.; Lewis, J. A. Laser-assisted Direct Ink Writing of Planar and 3D Metal Architectures. *Proc. Natl. Acad. Sci. U.S.A.* **2016**, *113*, 6137.

(32) Fantino, E.; Chiappone, A.; Roppolo, I.; Manfredi, D.; Bongiovanni, R.; Pirri Candido, F.; Calignano, F. 3D Printing of Conductive Complex Structures with In Situ Generation of Silver Nanoparticles. *Adv. Mater.* **2016**, *28*, 3712−3717.

(33) Zhu, Z.; Guo, S. Z.; Hirdler, T.; Eide, C.; Fan, X.; Tolar, J.; McAlpine Michael, C. 3D Printed Functional and Biological Materials on Moving Freeform Surfaces. *Adv. Mater.* **2018**, *30*, No. 1707495.

(34) Stankovich, S.; Dikin, D. A.; Dommett, G. H. B.; Kohlhaas, K. M.; Zimney, E. J.; Stach, E. A.; Piner, R. D.; Nguyen, S. T.; Ruoff, R. S. Graphene-based Composite Materials. *Nature* **2006**, *442*, 282.

(35) De Volder, M. F. L.; Tawfick, S. H.; Baughman, R. H.; Hart, A. J. Carbon Nanotubes: Present and Future Commercial Applications. *Science* **2013**, *339*, 535.

(36) Bao, W. S.; Meguid, S. A.; Zhu, Z. H.; Weng, G. J. Tunneling Resistance and Its Effect on the Electrical Conductivity of Carbon Nanotube Nanocomposites. *J. Appl. Phys.* **2012**, *111*, No. 093726.

(37) Wu, H. P.; Liu, J. F.; Wu, X. J.; Ge, M. Y.; Wang, Y. W.; Zhang, G. Q.; Jiang, J. Z. High Conductivity of Isotropic Conductive Adhesives Filled with Silver Nanowires. *Int. J. Adhes. Adhes.* **2006**, *26*, 617−621.

(38) Zhang, P.; Wyman, I.; Hu, J.; Lin, S.; Zhong, Z.; Tu, Y.; Huang, Z.; Wei, Y. Silver Nanowires: Synthesis Technologies, Growth Mechanism and Multifunctional Applications. *Mater. Sci. Eng., B* **2017**, *223*, 1−23.

(39) Li, B.; Ye, S.; Stewart, I. E.; Alvarez, S.; Wiley, B. J. Synthesis and Purification of Silver Nanowires To Make Conducting Films with a Transmittance of 99%. *Nano Lett.* **2015**, *15*, 6722−6726.

(40) Cauchy, X.; Klemberg-Sapieha, J. E.; Therriault, D. Synthesis of Highly Conductive, Uniformly Silver-coated Carbon Nanofibers by Electroless Deposition. *ACS Appl. Mater. Interfaces* **2017**, *9*, 29010−29020.
(41) Jiang, Y.; Xu, Z.; Huang, T.; Liu, Y.; Guo, F.; Xi, J.; Gao, W.; Gao, C. Direct 3D Printing of Ultralight Graphene Oxide Aerogel Microlattices. *Adv. Funct. Mater.* **2018**, *28*, No. 1707024.
(42) Guo, S. Z.; Gosselin, F.; Guerin, N.; Lanouette, A. M.; Heuzey, M. C.; Therriault, D. Solvent-cast Three-dimensional Printing of Multifunctional Microsystems. *Small* **2013**, *9*, 4118−4122.
(43) Passieux, R.; Guthrie, L.; Hosseini, R. S.; Lévesque, M.; Therriault, D.; Gosselin, F. P. Instability-assisted Direct Writing of Microstructured Fibers Featuring Sacrificial Bonds. *Adv. Mater.* **2015**, *27*, 3676−3680.
(44) Yan, B.; Gu, S.; Zhang, Y. Polylactide-based Thermoplastic Shape Memory Polymer Nanocomposites. *Eur. Polym. J.* **2013**, *49*, 366−378.
(45) Xu, B.; Fu, Y. Q.; Ahmad, M.; Luo, J. K.; Huang, W. M.; Kraft, A.; Reuben, R.; Pei, Y. T.; Chen, Z. G.; De Hosson, J. T. M. Thermomechanical Properties of Polystyrene-based Shape Memory Nanocomposites. *J. Mater. Chem.* **2010**, *20*, 3442−3448.
(46) Ge, Q.; Sakhaei, A. H.; Lee, H.; Dunn, C. K.; Fang, N. X.; Dunn, M. L. Multimaterial 4D Printing with Tailorable Shape Memory Polymers. *Sci. Rep.* **2016**, *6*, No. 31110.
(47) Yang, Y.; Chen, Y.; Wei, Y.; Li, Y. 3D Printing of Shape Memory Polymer for Functional Part Fabrication. *Int. J. Adv. Manuf. Technol.* **2016**, *84*, 2079−2095.
(48) Peng, Q.; Wei, H.; Qin, Y.; Lin, Z.; Zhao, X.; Xu, F.; Leng, J.; He, X.; Cao, A.; Li, Y. Shape-memory Polymer Nanocomposites with a 3D Conductive Network for Bidirectional Actuation and Locomotion Application. *Nanoscale* **2016**, *8*, 18042−18049.
(49) Zarek, M.; Layani, M.; Cooperstein, I.; Sachyani, E.; Cohn, D.; Magdassi, S. 3D Printing of Shape Memory Polymers for Flexible Electronic Devices. *Adv. Mater.* **2016**, *28*, 4449−4454.